

# Efficient Polarimetric Analysis of Accretion Disks around Kerr Black Holes

[arXiv:2308.15159](https://arxiv.org/abs/2308.15159)

Vladislav Loktev (University of Turku)

30.08.2023, Český Krumlov

**South Bohemian X-ray polarisation workshop**

IXPE GO proposals for BH XRBs and AGN

# Modeling the polarization spectrum

1. Geometry of the system
2. Local emission at the disk
3. Gravitational redshift and Doppler boosting
4. Light bending and rotation of the polarization frame

# Modeling the polarization spectrum

## Geometry

- Assume thin equatorial disk
- For a soft state disk around a Kerr BH, the inner radius of the disk depends on the spin parameter

## Redshift

- For the emission from the equatorial plane of the BH, the SR and GR redshift is computed analytically

## Local emission

- The radial emission pattern also depends on spin, null hypothesis (and our example) is a standard thin disk described in [Novikov & Thorne (1973)]
- As a simple local atmosphere model we can adopt Chandrasekhar's electron scattering atmosphere.

The audience is not supposed to pay too much attention to this corner of the slide

# Modeling the polarization spectrum

## Geometry

- Assume thin equatorial disk
- For a soft state disk around a Kerr BH, the inner radius of the disk depends on the spin parameter

## Redshift

- For the emission from the equatorial plane of the BH, the SR and GR redshift is computed analytically

## Local emission

- The radial emission pattern also depends on spin, null hypothesis (and our example) is a standard thin disk described in [Novikov & Thorne (1973)]
- As a simple local atmosphere model we can adopt Chandrasekhar's electron scattering atmosphere.

$$r_{\text{ISCO}} = \frac{1}{2} \left( 3 + Z_2 \pm \sqrt{(3 - Z_1)(3 + Z_1 + 2Z_2)} \right)$$

$$Z_1 = 1 + \sqrt[3]{1 - a^2} \left( \sqrt[3]{1 + a} + \sqrt[3]{1 - a} \right)$$

$$Z_2 = \sqrt{3a^2 + Z_1^2}.$$

# Modeling the polarization spectrum

## Geometry

- Assume thin equatorial disk
- For a soft state disk around a Kerr BH, the inner radius of the disk depends on the spin parameter

## Redshift

- For the emission from the equatorial plane of the BH, the SR and GR redshift is computed analytically

## Local emission

- The radial emission pattern also depends on spin, null hypothesis (and our example) is a standard thin disk described in [Novikov & Thorne (1973)]
- As a simple local atmosphere model we can adopt Chandrasekhar's electron scattering atmosphere.

$$T_{\text{eff}}^4(r) = \frac{3GM\dot{M}}{8\pi\sigma_{\text{SB}}R^3} f(r, a) = T_*^4 \frac{f(r, a)}{r^3},$$

$$F_{E'} = \frac{\pi}{f_{\text{col}}^4} B_{E'}(f_{\text{col}} T_{\text{eff}})$$

$$a_{\text{es}}(\zeta') = \frac{60}{143} (1 + 2.3 \cos \zeta' - 0.3 \cos^2 \zeta')$$

$$p_{\text{es}}(\zeta') = 0.1171 \frac{1 - \cos \zeta'}{1 + 3.582 \cos \zeta'}$$

# Modeling the polarization spectrum

## Geometry

- Assume thin equatorial disk
- For a soft state disk around a Kerr BH, the inner radius of the disk depends on the spin parameter

## Local emission

- The radial emission pattern also depends on spin, null hypothesis (and our example) is a standard thin disk described in [Novikov & Thorne (1973)]
- As a simple local atmosphere model we can adopt Chandrasekhar's electron scattering atmosphere.

## Redshift

- For the emission from the equatorial plane of the BH, the SR and GR redshift is computed analytically

$$\beta = \frac{\mathcal{F}}{\mathcal{B} \sqrt{\mathcal{D}}} \sqrt{\frac{1}{2r}}$$

$$g = E/E' = \gamma [\mathcal{X} + \mathcal{Y}\beta + (\mathcal{X}\beta + \mathcal{Y}) \cos \xi']$$

where

$$\mathcal{X} = \sqrt{\mathcal{D}/\mathcal{A}},$$

$$\mathcal{Y} = a / \sqrt{4r^4 \mathcal{A}},$$

$$\mathcal{A} = 1 + (r + 1) \frac{a^2}{4r^3}.$$

$$\mathcal{B} = 1 + \frac{a}{\sqrt{8r^3}},$$

$$\mathcal{D} = 1 - \frac{1}{r} + \frac{a^2}{4r^2},$$

$$\mathcal{F} = 1 - \frac{a}{\sqrt{2r^3}} + \frac{a^2}{4r^3}.$$

# Model: Light bending (Kerr)

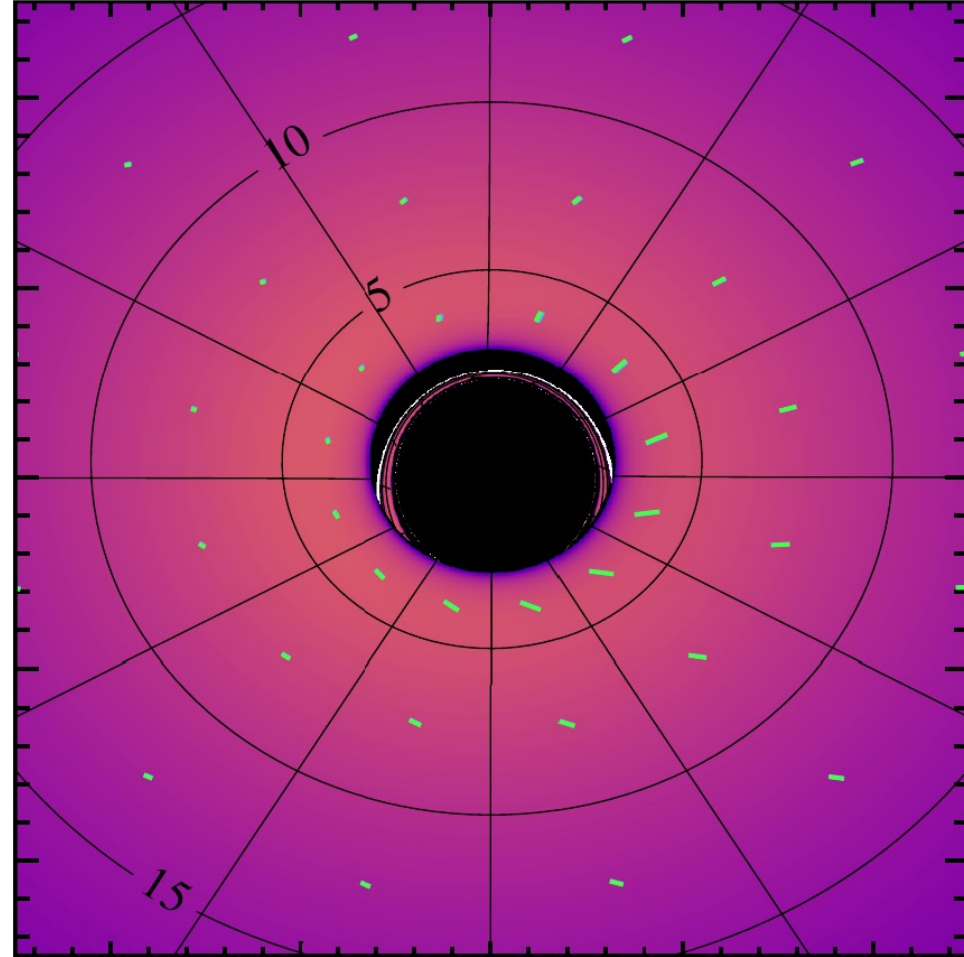
The Kerr metric

$$(g_{ab}) = \begin{pmatrix} 1 - \frac{2Mr}{\rho^2} & 0 & 0 & \frac{2Mra \sin^2 \theta}{\rho^2} \\ 0 & -\frac{\rho^2}{\Delta} & 0 & 0 \\ 0 & 0 & -\rho^2 & 0 \\ \frac{2Mra \sin^2 \theta}{\rho^2} & 0 & 0 & -\sin^2 \theta \left( r^2 + a^2 + \frac{2Mra^2 \sin^2 \theta}{\rho^2} \right) \end{pmatrix},$$

Solving geodesic equations,

$$\frac{du^a(\lambda)}{d\lambda} = -\Gamma_{bc}^a u^b u^c + f^a$$

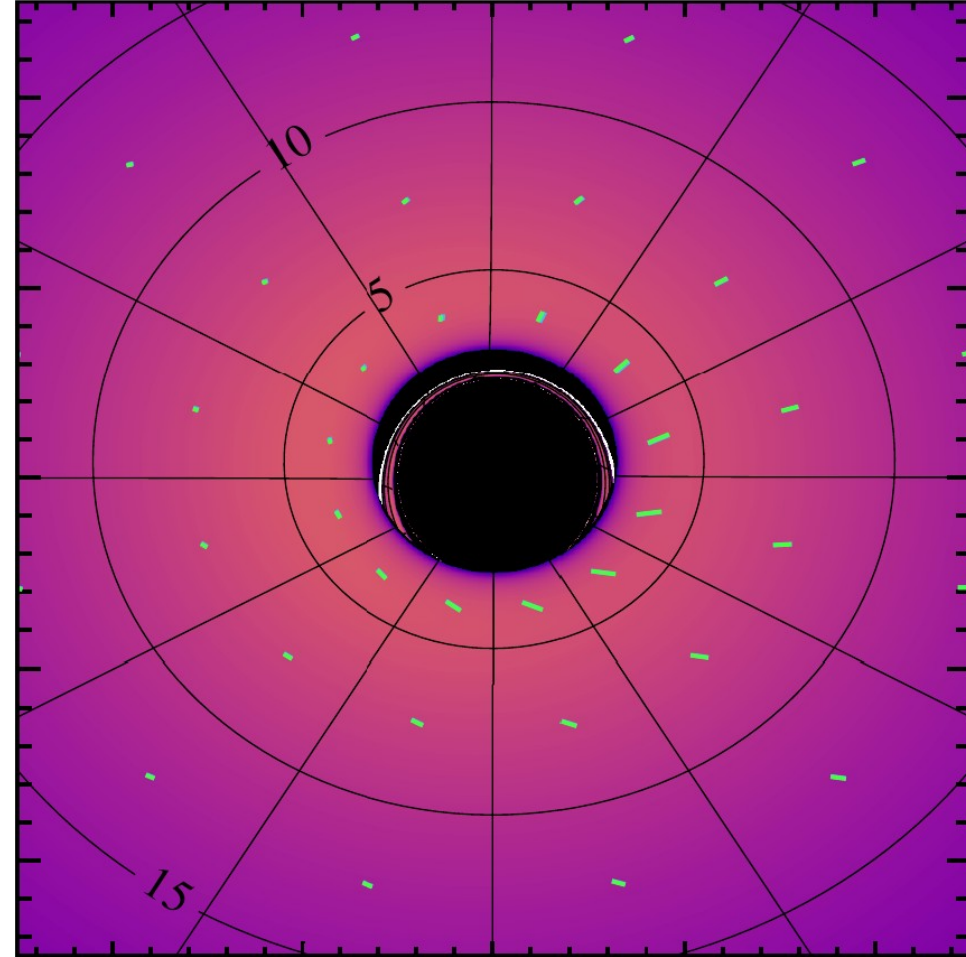
# Simple!



# Model: Light bending (Kerr)

$$\frac{du^a(\lambda)}{d\lambda} = -\Gamma_{bc}^a u^b u^c + f^a$$

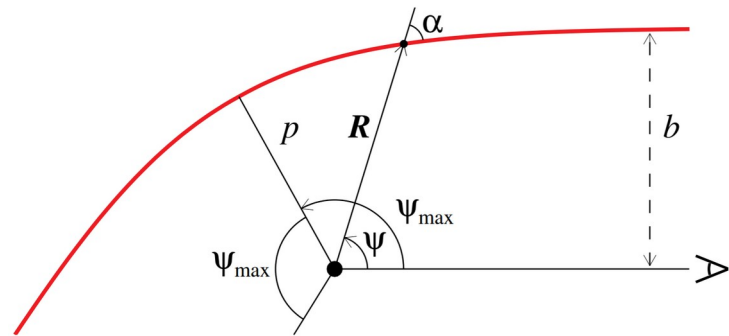
- We trace the geodesics from the observer **back** to the system
- There are **no analytical** solution to the geodesic equation. (slow)
- The result trajectories in the Kerr metric are **non-planar** due to frame-dragging.
- They are the most different from the zero-spin case at the **very vicinity** to the BH.





# Model: Light bending (Schwarzschild)

- The trajectories in the Schwarzschild metric are **planar**
- We do not compute the full trajectory but **explicitly** define the emission angle at the disk.
- We have **analytical** expressions and very good one-line approximation of the light bending
- The PA rotation is also expressed analytically (fast)



$$\psi(R, \alpha) = \int_R^\infty \frac{dr}{r^2} \left[ \frac{1}{b^2} - \frac{1}{r^2} \left( 1 - \frac{R_S}{r} \right) \right]^{-1/2}$$

$$x = (1 - u)y \left( 1 + \frac{u^2 y^2}{112} - \frac{e}{100} u y (\ln(1 - y/2) + y/2) \right),$$

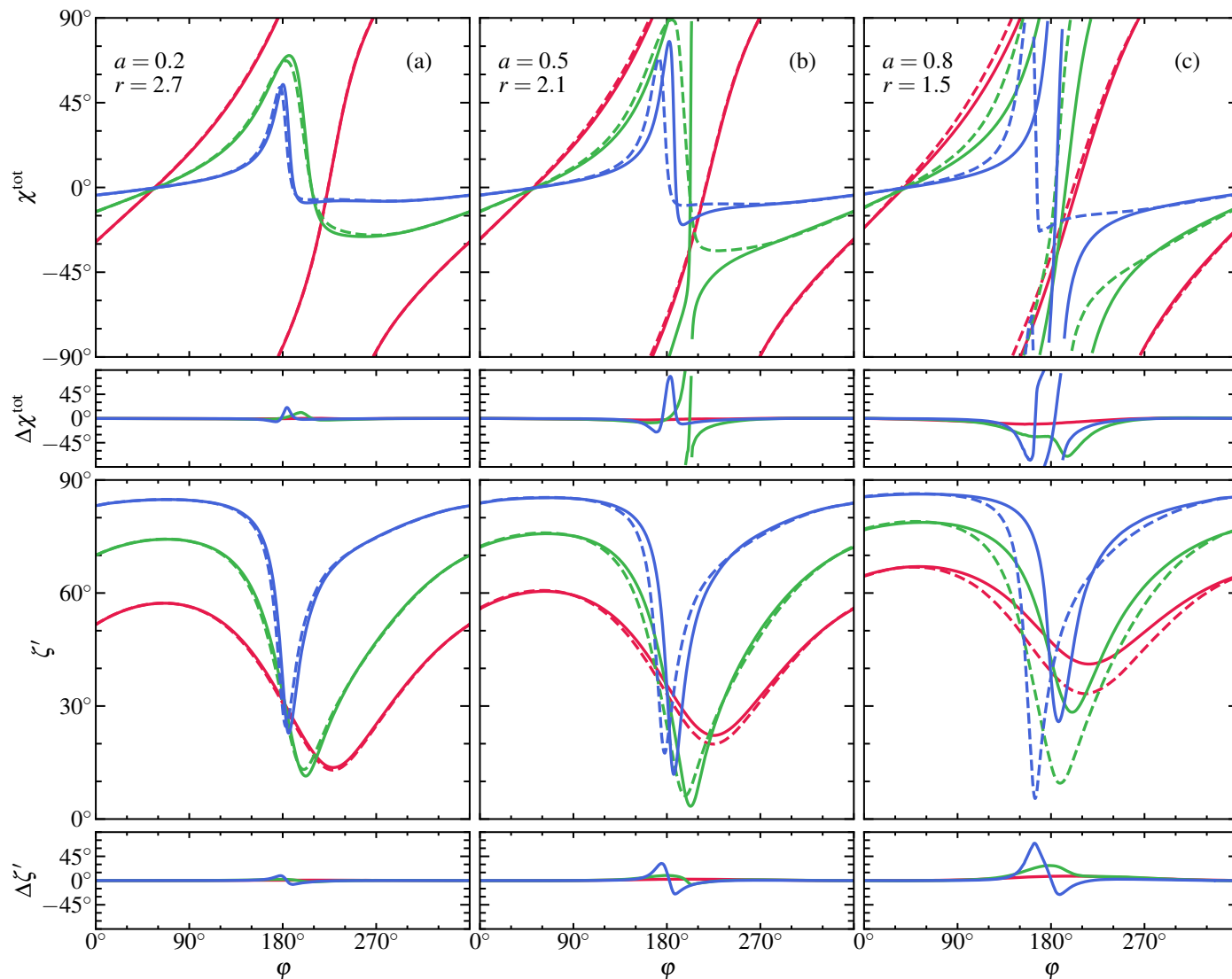
where  $x = 1 - \cos \alpha$ ,  $y = 1 - \cos \psi$ , and  $u = 2/r$ .

# Comparing our method with the numerical ray-tracing

\*using ARCMANCER [Pihajoki et. al. 2018]

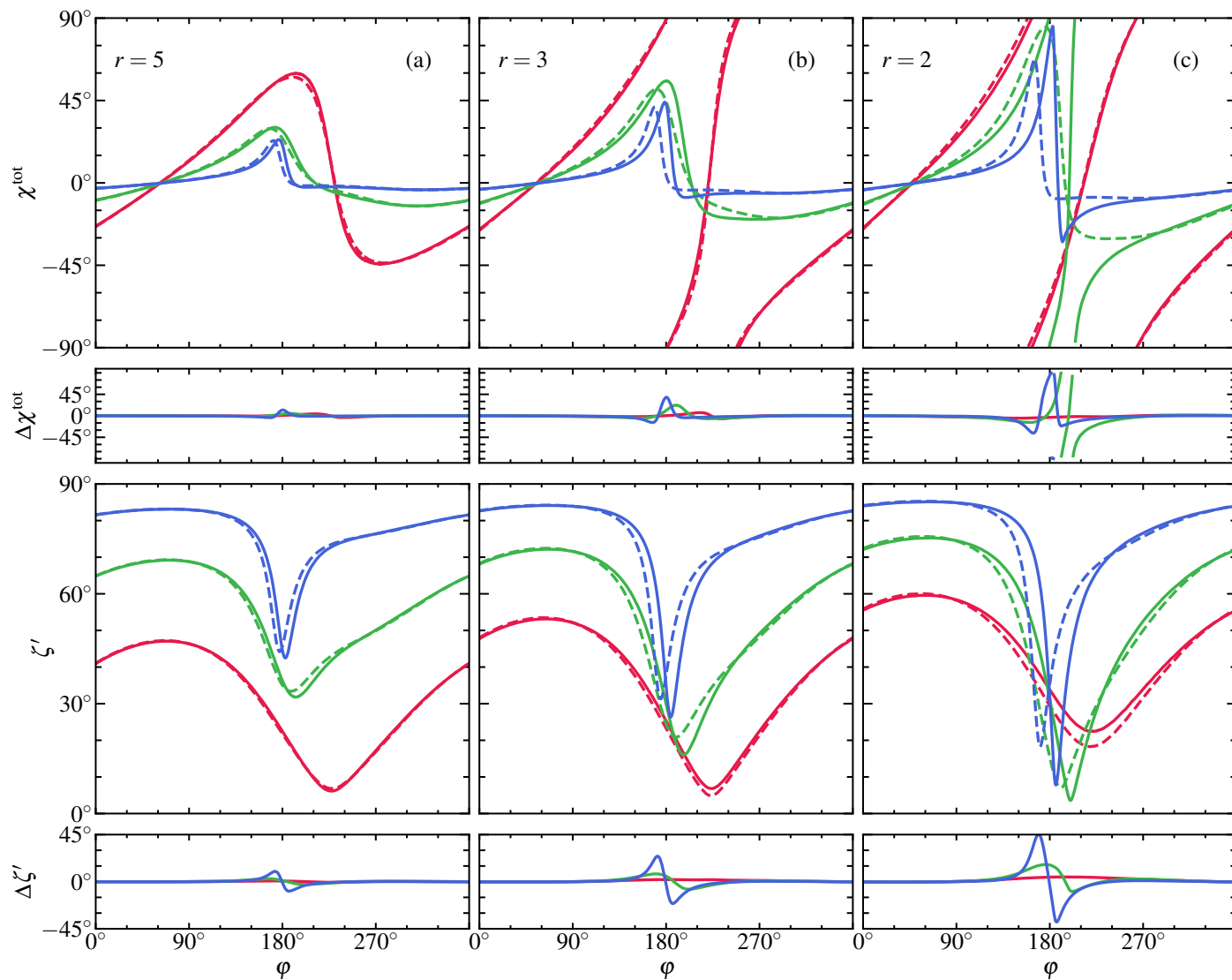
# Comparison: at ISCO

- PA rotation ( $\chi^{\text{tot}}$ ) and local emission angle ( $\zeta'$ ) as a function of azimuth at the ISCO for different BH spins and inclinations.
- The spin are  $a = 0.2, 0.5, 0.8$
- Inclinations are **30°**, **60°**, **80°**.
- The discrepancy between the methods is only significant for the light coming from the disk behind the BH, where the features are shifted by the Kerr frame-dragging



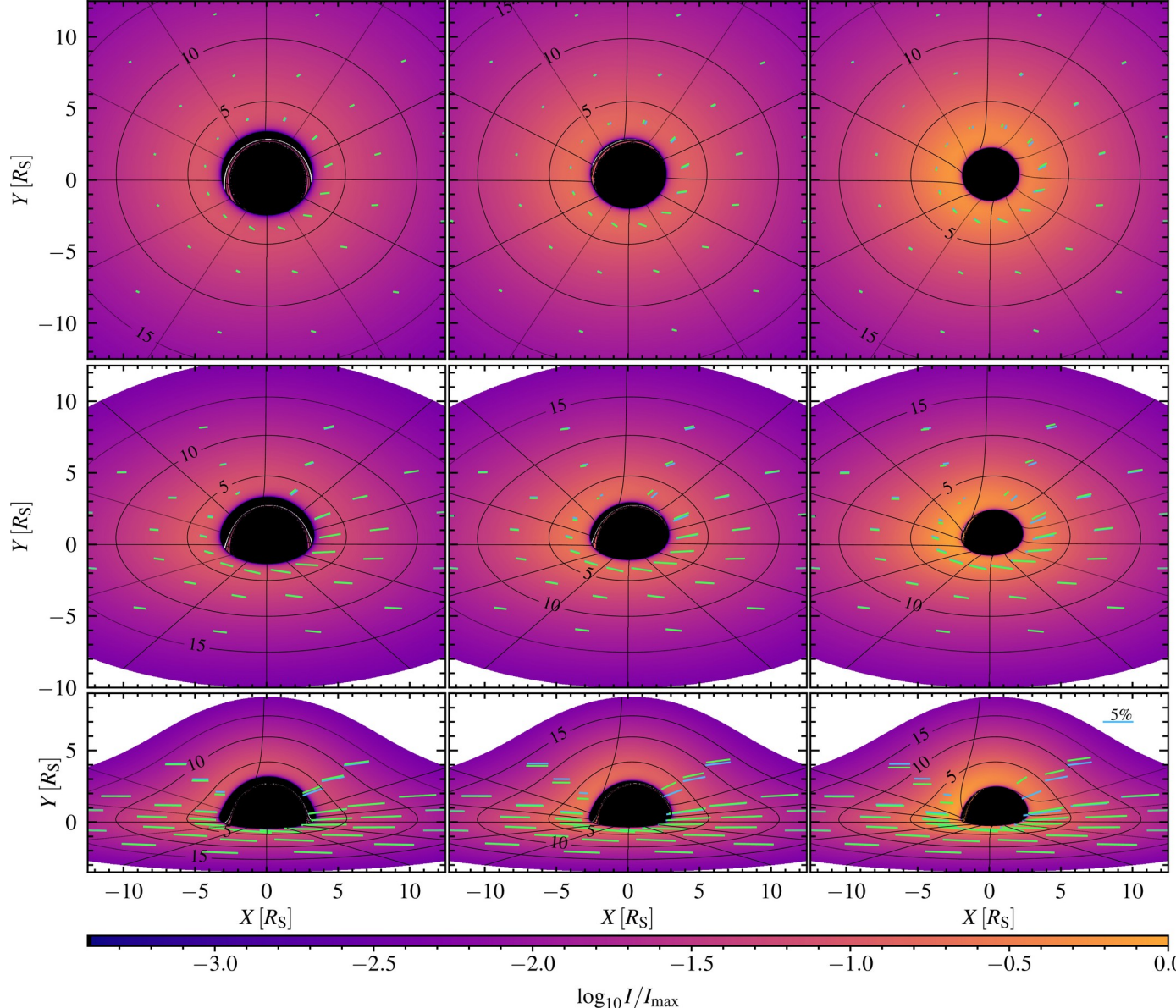
# Comparison: wider rings

- PA rotation ( $\chi^{\text{tot}}$ ) and local emission angle ( $\zeta'$ ) as a function of azimuth at different distances from the BH
- The spin is 0.8,
- At  $r = 2R_s, 3R_s, 5R_s$
- Inclinations are  $30^\circ$ ,  $60^\circ$ ,  $80^\circ$ .
- The difference is even less pronounced the further the emitting spot is from the BH



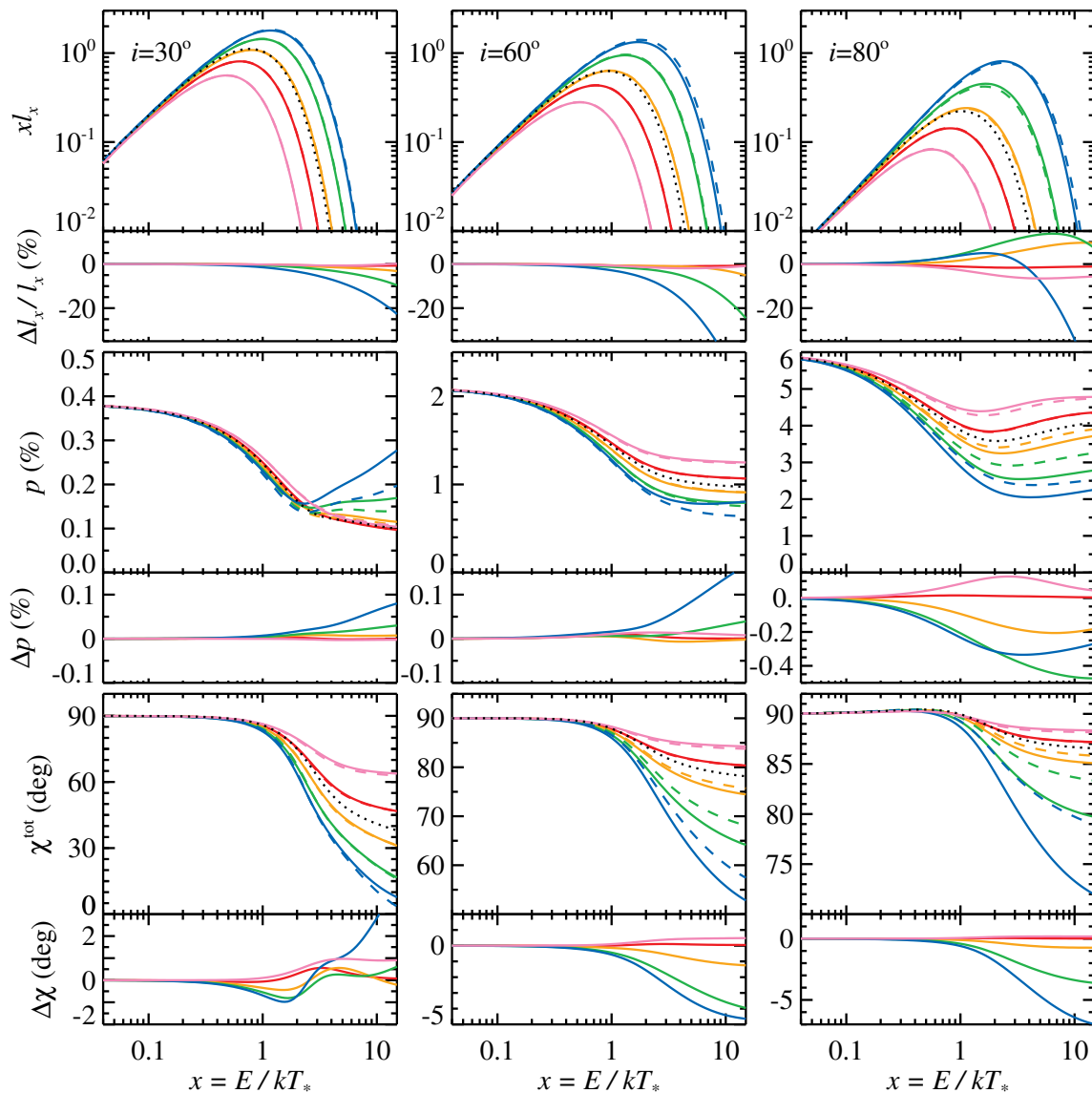
# Comparison: imaging

- Images of a thin disk, the inner part  $< 12 R_s$
- The spins are  $a = 0.2, 0.5, 0.8$  left to right
- Inclinations are  $30^\circ, 60^\circ, 80^\circ$  top to bottom
- The sticks show polarization computed with **analytical** and **numerical** method, and colormap shows the relative intensity.
- Unless lower right corner, the difference is hard to see.



# Comparison: spectra

- Polarization spectra: relative luminosity (top), PD (middle) and PA (bottom)
- Numerical (dashed) versus analytical (solid)
- The spins are  $a = -1, 0, 0.5, 0.8, 0.94$
- Inclinations are  $30^\circ, 60^\circ, 80^\circ$  left to right.
- For small inclinations the difference is very small.
- For  $a > 0.94$  the ISCO is below  $R_s$
- In general for  $a < 0.8$  the results are quite adequate.



# Conclusions

- We developed a fast method of computing polarization spectra from Kerr BH XRBs leveraging the Schwarzschild approximatoin of the light bending
- We tested our method against exact numerical ray-tracing techniques
- The results are accurate for inclinations  $< 80^\circ$  or spins  $< 0.8$
- Our method allows fast and flexible computation of polarization spectra.
- Our method is used to analyse the IXPE observations such as of CygX-1

# Conclusions

- We developed a fast method of computing polarization spectra from Kerr BH XRBs leveraging the Schwarzschild approximatoin of the light bending
- We tested our method against exact numerical ray-tracing techniques
- The results are accurate for inclinations  $< 80^\circ$  or spins  $< 0.8$
- Our method allows fast and flexible computation of polarization spectra.
- Our method is used to analyse the IXPE observations such as of CygX-1

Thank you



# Contribution of the secondary images

Contribution is less  
than 0.5% across  
all cases

